

Evaluating China's fossil-fuel CO₂ emissions from a comprehensive dataset of nine inventories

Pengfei Han^{1*}, Ning Zeng^{2*}, Tom Oda³, Xiaohui Lin⁴, Monica Crippa⁵, Dabo Guan^{6,7}, Greet Janssens-Maenhout⁵, Xiaolin Ma⁸, Zhu Liu^{6,9}, Yuli Shan¹⁰, Shu Tao¹¹, Haikun Wang⁸, Rong Wang^{11,12}, Lin Wu⁴, Xiao Yun¹¹, Qiang Zhang¹³, Fang Zhao¹⁴, Bo Zheng¹⁵

¹State Key Laboratory of Numerical Modeling for Atmospheric Sciences and Geophysical Fluid Dynamics, Institute of Atmospheric Physics, Chinese Academy of Sciences, Beijing, China

²Department of Atmospheric and Oceanic Science, and Earth System Science Interdisciplinary Center, University of Maryland, College Park, Maryland, USA

³Goddard Earth Sciences Research and Technology, Universities Space Research Association, Columbia, MD, United States

⁴State Key Laboratory of Atmospheric Boundary Layer Physics and Atmospheric Chemistry, Institute of Atmospheric Physics, Chinese Academy of Sciences, Beijing, China

⁵European Commission, Joint Research Centre (JRC), Directorate for Energy, Transport and Climate, Air and Climate Unit, Ispra (VA), Italy

⁶Department of Earth System Science, Tsinghua University, Beijing, China

⁷Water Security Research Centre, School of International Development, University of East Anglia, Norwich, UK

⁸State Key Laboratory of Pollution Control and Resource Reuse, School of the Environment, Nanjing University, Nanjing, China

⁹Tyndall Centre for Climate Change Research, School of International Development, University of East Anglia, Norwich, UK

¹⁰Energy and Sustainability Research Institute Groningen, University of Groningen, Groningen 9747 AG, Netherlands

¹¹Laboratory for Earth Surface Processes, College of Urban and Environmental Sciences, Peking University, Beijing, China

¹²Department of Environmental Science and Engineering, Fudan University, Shanghai, China

¹³Ministry of Education Key Laboratory for Earth System Modeling, Department of Earth System Science, Tsinghua University, Beijing, China

¹⁴Key Laboratory of Geographic Information Science (Ministry of Education), School of Geographic Sciences, East China Normal University, Shanghai, China

¹⁵Laboratoire des Sciences du Climat et de l'Environnement, CEA-CNRS-UVSQ, UMR8212, Gif-sur-Yvette, France

Correspondence to: Pengfei Han (pphan@mail.iap.ac.cn); Ning Zeng (zeng@umd.edu)

Abstract. China's fossil-fuel CO₂ (FFCO₂) emissions accounted for approximately 28% of the global total FFCO₂ in 2016. An accurate estimate of China's FFCO₂ emissions is a prerequisite for global and regional carbon budget analyses and the monitoring of carbon emission reduction efforts. However, significant uncertainties and discrepancies exist in estimations of China's FFCO₂ emissions due to a lack of detailed traceable emission factors (EF) and multiple statistical data sources. Here, we evaluated China's FFCO₂ emissions from nine published global and regional emission datasets. These datasets show that the total emissions increased from 3.4 (3.0-3.7) in 2000 to 9.8 (9.2-10.4) Gt CO₂ yr⁻¹ in 2016. The variations in these estimates were largely due to the different EF (0.491-0.746 t C per t of coal) and activity data. The large-scale patterns of gridded emissions showed a reasonable agreement with high emissions being concentrated in major city clusters, and the standard

deviation mostly ranged from 10-40% at the provincial level. However, patterns beyond the provincial scale varied significantly, with the top 5% of the grid-level accounting for 50-90% of total emissions in these datasets. Our findings highlight the significance of using locally measured EF for Chinese coal. To reduce uncertainty, we recommend using physical CO₂ measurements and use these values for datasets validation, key input data sharing (e.g., point sources) and finer resolution validations at various levels.

Keywords: fossil-fuel CO₂ emissions, spatial disaggregation, emission factor, activity data, comprehensive dataset

1 Introduction

Anthropogenic emissions of carbon dioxide (CO₂) is one of the major accelerators of global warming (IPCC, 2007). Global CO₂ emissions from fossil fuel combustion and industry processes increased to 36.23 Gt CO₂ yr⁻¹ in 2016, with a mean growth rate of 0.62 Gt CO₂ yr⁻¹ over the last decade (Le Quéré et al., 2018). In 2006, China became the world's largest emitter of CO₂ (Jones, 2007). CO₂ emissions from fossil fuel combustion and cement production in China were 9.9 Gt CO₂ in 2016, accounting for approximately 28% of all global fossil-fuel based CO₂ emissions (Le Quéré et al., 2018; IPCC AR5, 2013). To avoid the potential adverse effects from climate change (Zeng et al., 2008; Qin et al., 2016), the Chinese government has pledged to peak its CO₂ emissions by 2030 or earlier and to reduce CO₂ emissions per unit gross domestic product (GDP) by 60-65%, less than the 2005 levels (SCIO, 2015). Thus, an accurate quantification of China's CO₂ emissions is the first step toward understanding its carbon budget and making carbon control policy.

The total emission estimates for China are thought to be uncertain or biased due to the lack of reliable statistical data and/or the use of generic emission factors (EF) (e.g., (Guan et al., 2012); (Liu et al., 2015b)). National and provincial data-based inventories use activity data from different sources. The Carbon Dioxide Information Analysis Center (CDIAC) uses national energy statistics from the United Nations (UN) (Andres et al., 2012), and both the Open-Data Inventory for Anthropogenic Carbon Dioxide (ODIAC) and Global Carbon Project (GCP) mainly use CDIAC total estimates, and thus, they are identical in time series (Le Quéré et al., 2018; Oda et al., 2018). The Emissions Database for Global Atmospheric Research (EDGAR) and Peking University CO₂ (PKU-CO₂, hereafter named PKU) derive emissions from the energy balance statistics of the International Energy Agency (IEA) (Janssens-Maenhout et al., 2019a; Wang et al., 2013). In contrast, provincial data-based inventories developed within China all use the provincial energy balance sheet from the China Energy Statistics Yearbook (CESY), National Bureau of Statistics of China (NBS) (Cai et al., 2018; Liu et al., 2015a; Liu et al., 2013; Shan et al., 2018). There are generally four sources of EF, i.e., 1) The Intergovernmental Panel on Climate Change (IPCC) default values, which have been adopted by ODIAC and EDGAR (Andres et al., 2012; Janssens-Maenhout et al., 2019b; Oda et al., 2018); 2) National Development and Reform Commission (NDRC) (NDRC, 2012b); 3) China's National Communication, which reports to the United Nations Framework Convention on Climate Change (UNFCCC) (NDRC, 2012a); and 4) The China Emission Accounts and Datasets (CEADs) EF, which are locally optimized through large sample measurements (Liu et al.,

70 2015b). The existing estimates of global total FFCO₂ emissions are comparable in magnitude, with an uncertainty that is generally within $\pm 10\%$ (Le Quéré et al., 2018; Oda et al., 2018). However, there are significant differences in these values at the national scale (Marland et al., 2010; Olivier et al., 2014), with the uncertainty ranging from a few percent to more than 50% in the estimated emissions for individual countries (Andres et al., 2012; Boden et al., 2016; Oda et al., 2018).

Along with total emissions estimates, the spatial distribution of emissions is important for several reasons: 1) Spatial gridded products enhance our basic understanding of CO₂ emissions; 2) spatial distributions are key inputs (as priors) for transport and data assimilation models, which influence the carbon budget (Bao et al., 2020); and 3) spatial distributions can be used for policy making toward emissions reductions and can provide useful information for the deployment of instruments in emissions monitoring for high-emissions areas recognized by multiple inventories (Han et al., 2020). At the global level, gridded emissions datasets are often based on the disaggregation of country-scale emissions (Janssens-Maenhout et al., 80 2017; Wang et al., 2013). Thus, gridded emissions data are subjected to errors and uncertainties due to total emissions calculations and emissions spatial disaggregation (Andres et al., 2016; Oda et al., 2018; Oda and Maksyutov, 2011). For example, the Carbon Dioxide Information Analysis Center (CDIAC) distributes national energy statistics at a resolution of $1^\circ \times 1^\circ$ using population density as a proxy (Andres et al., 2016; Andres et al., 2011). Further, to improve the spatial resolution of the emissions inventory, the Open-Data Inventory for Anthropogenic Carbon dioxide (ODIAC) distributes national emissions based on CDIAC and BP statistics with satellite nighttime lights and power plant emissions (Oda et al., 2018; Oda and Maksyutov, 2011). EDGAR derives emissions from the energy balance statistics of the International Energy Agency (IEA) and obtains country-specific activity datasets from BP plc, United States Geological Survey (USGS), World Steel Association, Global Gas Flaring Reduction Partnership (GGFR)/U.S. National Oceanic and Atmospheric Administration (NOAA) and International Fertilizer Association (IFA). Gridded emissions maps at a resolution of $0.1^\circ \times 0.1^\circ$ are produced 85 using spatial proxy data based on population density, traffic networks, nighttime lights and point sources, as described in Janssens-Maenhout et al. (2017). Based on subnational fuel, population and other geographically resolved data, a high-resolution inventory of global CO₂ emissions was developed at Peking University (Wang et al., 2013).

To accurately calculate emissions, a series of efforts have been conducted to quantitatively evaluate China's CO₂ emissions using national or provincial activity data, local EF and detailed datasets of point sources (Cai et al., 2018; Li et al., 95 2017; Wang et al., 2013). The China High Resolution Emission Database (CHRED) was developed by Cai et al. (2018) and Wang et al. (2014) based on provincial statistics, traffic network, point sources and industrial and fuel-specific EF. CHRED was featured based on its exclusive point source data from 1.58 million industrial enterprises from the First China Pollution Source Census. The Multiresolution Emission Inventory for China (MEIC) was developed by Zhang et al. (2007), Lei et al. (2011) and Liu et al. (2015a) at Tsinghua University through the integration of provincial statistics, unit-based power plant 100 emissions, population density, traffic networks and EF (Li et al., 2017; Zheng et al., 2018b; Zheng et al., 2018a). The MEIC

uses the China Power Emissions Database (CPED), in which the unit-based approach is used to calculate emissions for each coal-fired power plant in China with detailed unit-level information (e.g., coal use, geographical coordinates). Regarding mobile emissions sources, a high-resolution mapping approach is adopted to constrain vehicle emissions using a county-level activity database. CEADs was constructed by (Shan et al., 2018;Shan et al., 2016) and Guan et al. (2018) based on different levels of inventories to provide emissions at the national and provincial scales. CEADs uses coal EF from large-sample measurements (602 coal samples and samples from 4,243 coal mines), which are assumed to be more accurate than the IPCC default EFs.

However, regardless of these efforts, China's CO₂ emissions remain uncertain due to the large discrepancy among current estimates, of which the difference ranges from 8-24% of total estimates (Shan et al., 2018;Shan et al., 2016). Several studies have undertaken efforts to quantify the possible uncertainty in China's FFCO₂, such as differences due to estimation approaches (Berezin et al., 2013), energy statistics (Hong et al., 2017;Han et al., 2020), spatial scales (Wang and Cai, 2017) and point source data. Importantly, the authors note that the lack of a comprehensive understanding and comparison of the potential uncertainty in estimates of China's FFCO₂, including spatial, temporal, proxy and magnitude components, cause Chinese emissions data to be more uncertain, and thus, it is important to present, analyze and explain such differences among inventories.

Here, we evaluated the uncertainty in China's FFCO₂ estimates by synthesizing global gridded emissions datasets (ODIAC, EDGAR and PKU) and China-specific emission maps (CHRED, MEIC and the Nanjing University CO₂ (NJU) emission inventory). Moreover, several other inventories were used in the evaluation analysis, such as the Global Carbon Budget from the Global Carbon Project and the National Communication on Climate Change of China (NCCC).

The aims of this study were to: 1) Quantify the magnitude and the uncertainty in China's FFCO₂ estimates using the spread of values from state-of-the-art inventories; 2) identify the spatiotemporal differences of China's FFCO₂ emissions among the existing emission inventories and explore the underlying reasons for such differences. To our knowledge, this is the first comprehensive evaluation of the most up-to-date and predominantly publicly available carbon emission inventories for China.

2. Emissions data

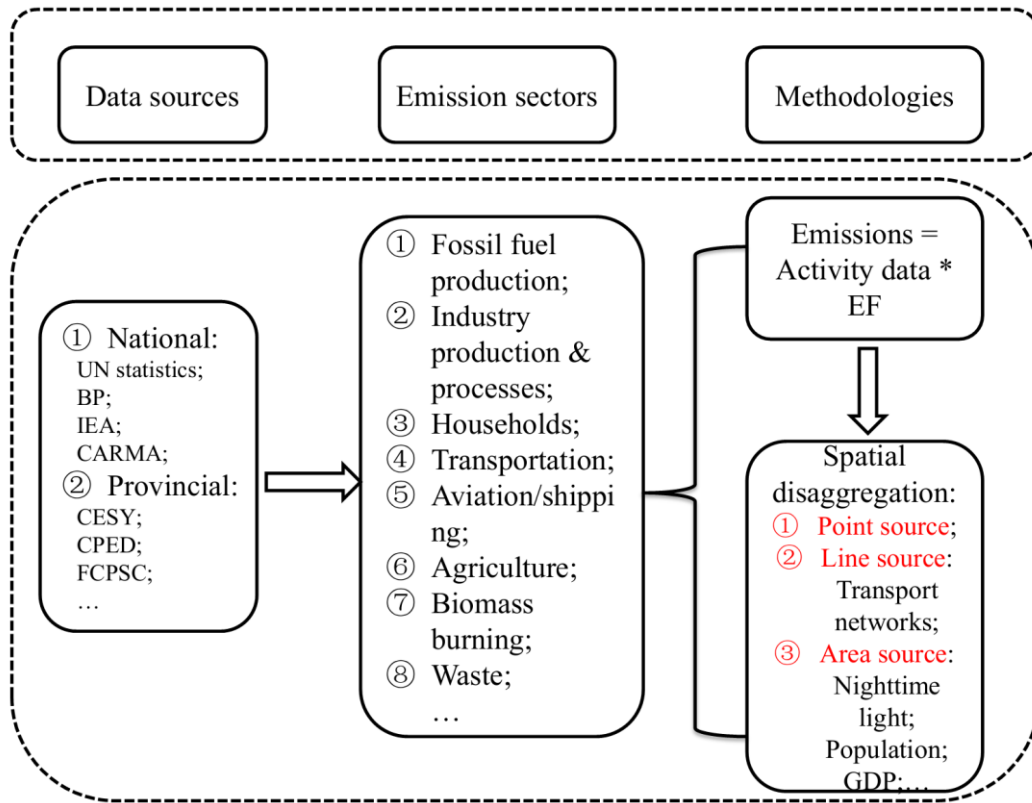
An evaluation analysis was conducted from 9 inventories including six gridded datasets (listed in Table 1, ODIAC, EDGAR, PKU, CHRED, MEIC, and NJU) and three other datasets (GCP/CDIAC, CEADs, and NCCC) containing statistical data. We selected the year 2012 for spatial analysis because this is the most recent year available for all the gridded datasets and also because 2012 was a peak year of emissions due to the strong reductions following the impact of the 12th-Five-Year-Plan.

Specifically, the global fossil fuel CO₂ emissions datasets included the year 2017 version of ODIAC (ODIAC2017), version

4.3.2 of EDGAR (EDGARv4.3.2) and PKU-CO₂, all of which use the Carbon Monitoring for Action (CARMA) as the point source. The China-specific emissions data used were from 2007 from CHRED, MEIC v1.3 and NJU-CO₂ v2017, all of which use China Energy Statistical Yearbook (CESY) activity data. Moreover, three inventories were used as references, i.e., GCP/CDIAC, CEADs and NCCC, because GCP and ODIAC use CDIAC for the majority of the years, except the most-recent two years, which were extrapolated using BP data. These three inventories were treated as inventory in a time series comparison. Data were collected from the official websites of ODIAC, EDGAR, PKU, and six tabular statistical datasets and were also acquired from the authors who developed CHRED, MEIC and NJU. See the supporting information for more details of the data sources and the methodology used for each dataset.

3. Methodology for the evaluation of multiple datasets

We evaluated the abovementioned datasets from three aspects: data sources, boundary (emission sectors) and methodology (Figure 1, Table 1 and S1, S2). In regard to the data source, there are two levels: national data, such as UN or IEA statistics, and provincial-level data, such as CESY. The emission sectors mainly include fossil fuel production, industry production and processes, households, transportation, aviation/shipping, agriculture, natural biomass burning from wild fires and the waste from these datasets; Table S1 lists the sectors included in each inventory. In addition, for methodology, the analysis of the inventories includes the total estimates (activity data and EF) aspect and the spatial disaggregation of point, line and area sources. Fig. 1 shows the conceptual procedure followed for the total emissions estimates and how the gridded maps were produced for all the inventories, and thus, it is important to know the differences in the activity data, EF and spatial proxy data and spatial disaggregation methods used by previous scholars to understand the differences among the inventories in regard to total emissions estimates and spatial characteristics.



150

Figure 1 Conceptual diagram for data evaluation based on data sources, emission sectors and methodologies.

The preprocessing of six gridded CO₂ emission datasets included several steps, which are described as follows. First, global maps of CO₂ emissions (i.e., ODIAC, EDGAR and PKU) were reprojected using the Albers Conical Equal Area projection (that of CHRED). Next, the nearest neighbor algorithm was used to resample different spatial resolutions into a pixel size of 10 km×10 km, and this method takes the value from the cell closest to the transformed cell as the new value. Second, the national total emissions were derived using the ArcGIS zonal statistics tool from CHRED, while the other emissions were from tabular data provided by the data owners. Finally, the grids for each inventory were sorted in ascending order and then plotted on a logarithmic scale to represent the distribution of emissions. To identify the contribution of high emission grids, emissions at the grid level that exceeded 50 kt CO₂ yr⁻¹ km⁻² and the top 5% emitting grids were selected for analysis.

155

Table 1 General information of the emissions datasets*

Data	ODIAC2017	EDGARv432	PKU	CHRED	MEIC	NJU	CEADs	GCP/CDIAC	NCCC
Domain	Global	Global	Global	China	China	China	China	Global	China
Temporal coverage	2000-2016	1970-2012	1960-2014	2007, 2012	2000-2016	2000-2015	1997-2015	1959-2018	2005, 2012, 2014
Temporal resolution	Monthly	Annual	Monthly	Biennially or triennially	Monthly	Annual	Annual	Annual	Annual
Spatial resolution	1 km	0.1 degree	0.1 degree	10 km	0.25 degree	0.25 degree	N/A	N/A	N/A
Emission estimates	Global & National	Global & National	Global & National	National & Provincial	National & Provincial	National & Provincial	National & Provincial	Global & National	National
Emission factor for raw coal (tC per t of coal)	0.746	0.713	0.518	0.518	0.491	0.518	0.499	0.746	0.491
Uncertainty	17.5% (95% CI)	±15%	±19% (95% CI)	±8%	±15%	7-10% (90% CI)	-15% - 25% (95% CI)	17.5% (95% CI)	5.40%
Point	CARMA	CARMA3.0	CARMA2.0	FCPSC	CPED	CEC;A	N/A	N/A	N/A

source	2.0					CC;CC TEN			
Line source	N/A	the OpenStreetMap and OpenRailwayMap, Int. aviation and bunker	N/A	The national road, railway, navigation network, traffic flows	Transport networks	N/A	N/A	N/A	N/A
Area source	Nighttime light	Population density, nighttime light	Vegetation and population density, nighttime light	Population density, land use, human activity	Population density, land use	Population density, GDP	N/A	N/A	N/A
Version name	ODIAC2017	EDGARv4.3.2_FT2016, EDGARv4.3.2	PKU-CO2-v2	CHRED	MEIC v.1.3	NJU-CO ₂ v2017	CEADs	N/A	N/A
Year published/updated	2018	2017	2016	2017	2018	2017	2017	2019	2018

Data sources	http://db.cger.nies.go.jp/dataset/ODI/AC/	http://edgar.jrc.ec.europa.eu/overview.php?v=432_GHG&SECURE=123	http://inventory.pku.edu.cn/download/download.html	Data developer	Data developer	Data developer	http://www.cead.s.net/(registration/required)	https://www.globalcarbonproject.org/carbonbudget/19/data.htm	https://unfccc.int/sites/default/files/resource/China2BUR_English.pdf
References	Oda (2018)	Janssens-Maenhout (2017)	Wang et al., 2013	Cai et al. (2018); Wang et al. (2014)	Zheng (2018); Liu et al. (2015)	Liu (2013)	Shan et al. (2018)	Friedlingstein et al. (2019)	NCCC (2018)

161 * CI: Confidence interval; FCPSC: the First China Pollution Source Census; CPED: China Power Emissions Database; CEC: Commission for Environmental Cooperation;

162 ACC: China Cement Almanac; CCTEN: China Cement Industry Enterprise Indirectory; GDP: Gross domestic product; N/A: Not available.

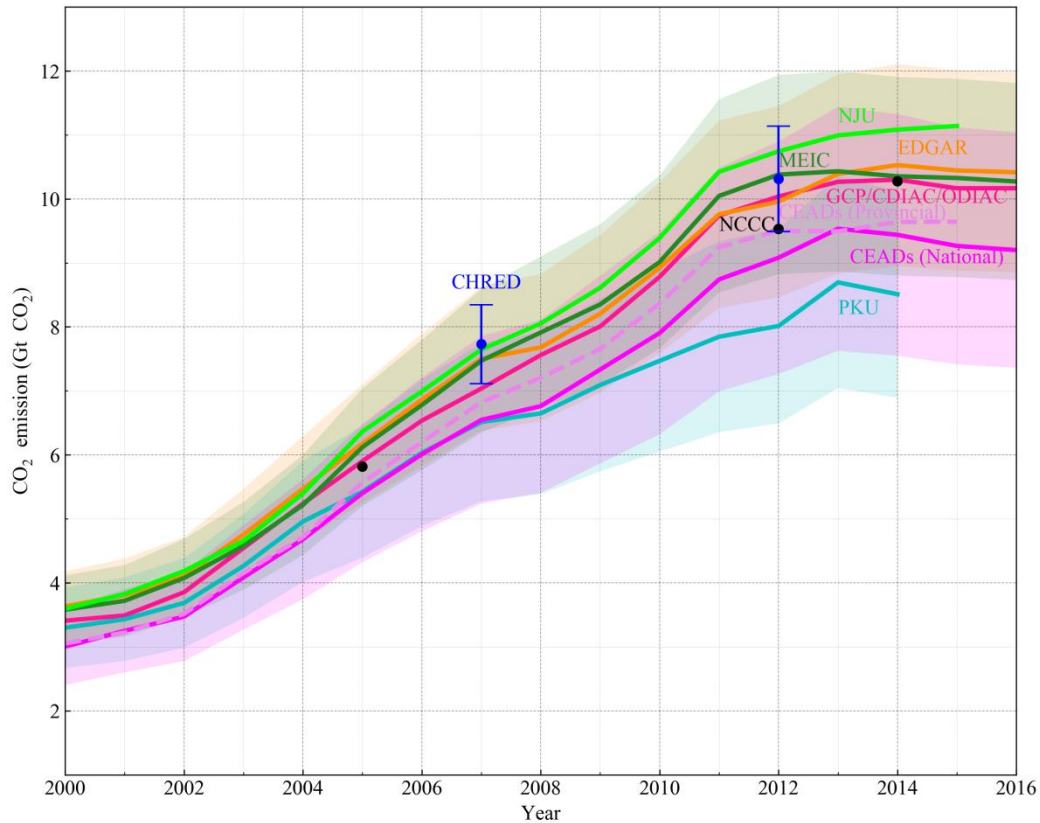
4. Results

4.1 Total emissions and recent trends

165 The interannual variations of China's CO₂ emissions from 2000 to 2016 were evaluated from six gridded emission maps and three national total inventories (Figure 2). All the datasets show a significant increasing trend in the period of 2000 to 2013 from 3.4 to 9.9 Gt CO₂. The range of the nine estimates increased simultaneously from 0.7 to 2.1 Gt CO₂ (both are 21% of the corresponding years' total emissions). In the second period (from 2013 to 2016), the temporal variations mostly levelled off or even decreased. Specifically, the emissions estimated from PKU and CEADs showed a slight downward trend, even
170 though they used independent activity data from IEA (2014) and National Bureau of Statistics (2016), and this downward trend was attributed to changes in the industrial structure, improved combustion efficiency, emissions control and slowing economic growth (Guan et al., 2018;Zheng et al., 2018a).

There is a large discrepancy among the current estimates, ranging from 8.0 to 10.7 Gt CO₂ in 2012. NJU had the highest emissions during the periods of 2005-2015, followed by EDGAR, MEIC and CDIAC/GCP/ODIAC, while CEADs (National)
175 and PKU were significantly lower (Figure 2). These discrepancies are mainly because of three reasons: 1) the EF for raw coal was greater for EDGAR and ODIAC than the other databases. The EFs were different for different fossil fuel types and cement production (Table S2). Because coal consumption constituted 70-80% of total emissions, the coal EF was more significant than the others. The EFs were different for the three major fossil fuel types (raw coal, oil and natural gas) and cement production (Table 1 and S2). In addition, the EFs were obtained from either the IPCC default values or local
180 optimized values from different sources. The EFs do not change over time in these inventories, although they should, due to the unavailability of EFs over time; 2) differences in activity data, i.e., NJU, MEIC and CEADs (Provincial) use provincial data from CESY (2016), while CEADs (National) and PKU use national data from CESY (2016) and IEA (2014), respectively (Table 1 and S1), such that the sum of provincial emissions is higher than the national total; and 3) differences in emission definitions (Table 1 and S1, emissions sectors). Although we tried to ensure that these datasets would be as
185 comparable as possible, minor differences in emissions sources (sectors) remained. For example, EDGAR contains abundant industry process-related emissions, whereas CEADs only considers cement production (Janssens-Maenhout et al., 2019b). EDGAR and MEIC have similar trends, except for their magnitudes, and MEIC is usually greater than EDGAR. This is a combined effect of the above three reasons. Moreover, MEIC uses provincial energy data from CESY (2016), whereas EDGAR uses national-level data from IEA (2014). However, MEIC's EF is lower than that of EDGAR. These opposing
190 effects bring the datasets closer in magnitude. Both the gridded products (ODIAC, EDGAR, MEIC and NJU) and national inventory (GCP/CDIAC) show small differences in the magnitude of total emissions estimates and trends from 2000-2007,

where the differences in magnitude increase gradually from 2008 onward. Although the range increases with time, the relative difference remains at approximately 21% of the corresponding years' total estimates, indicating potentially systematic differences, such as the fact that EFs remain stable.



195

Figure 2. China's total FFCO₂ emissions from 2000 to 2016. The emissions are from the combustion of fossil fuels and cement production from different sources (EDGARv4.3.2_FT2016 includes international aviation and marine bunkers emissions). To maintain comparability and avoid differences resulting from emissions disaggregation (e.g., Oda et al. (2018)), the values of the six gridded emission inventories are tabular data provided by the data developers before spatial disaggregation. Prior to 2014, GCP data were taken from CDIAC, and those from 2015-2016 were calculated based on BP data and the fraction of cement production emissions in 2014. The shaded area (error bar for CHRED) indicates uncertainties from the coauthors' previous studies (See Table 1).

200

4.2 Spatial distribution of FFCO₂ emissions

The evaluation of spatially explicit FFCO₂ emissions is fundamentally limited by the lack of direct physical measurements at the grid scale (e.g., (Oda et al., 2018)). Thus, we attempted to characterize the spatial patterns of China's carbon emissions by presenting the available emissions estimates. We compared six gridded products, including ODIAC, EDGAR, PKU, CHRED, MEIC and NJU, for the year 2012, which was the most recent year for which all six datasets were available. Spatially, the CO₂ emissions from the different datasets are concentrated in eastern China (Figure 3). The high-emission areas were mostly distributed in city clusters (e.g., BeijingTianjin-Hebei (Jing-Jin-Ji), the Yangtze River Delta and the Pearl River Delta) and densely populated areas (e.g., the North China Plain, the Northeast China Plain and Sichuan Basin). These major spatial patterns are primarily due to the use of spatial proxy data and are also in accordance with previous studies

205

210

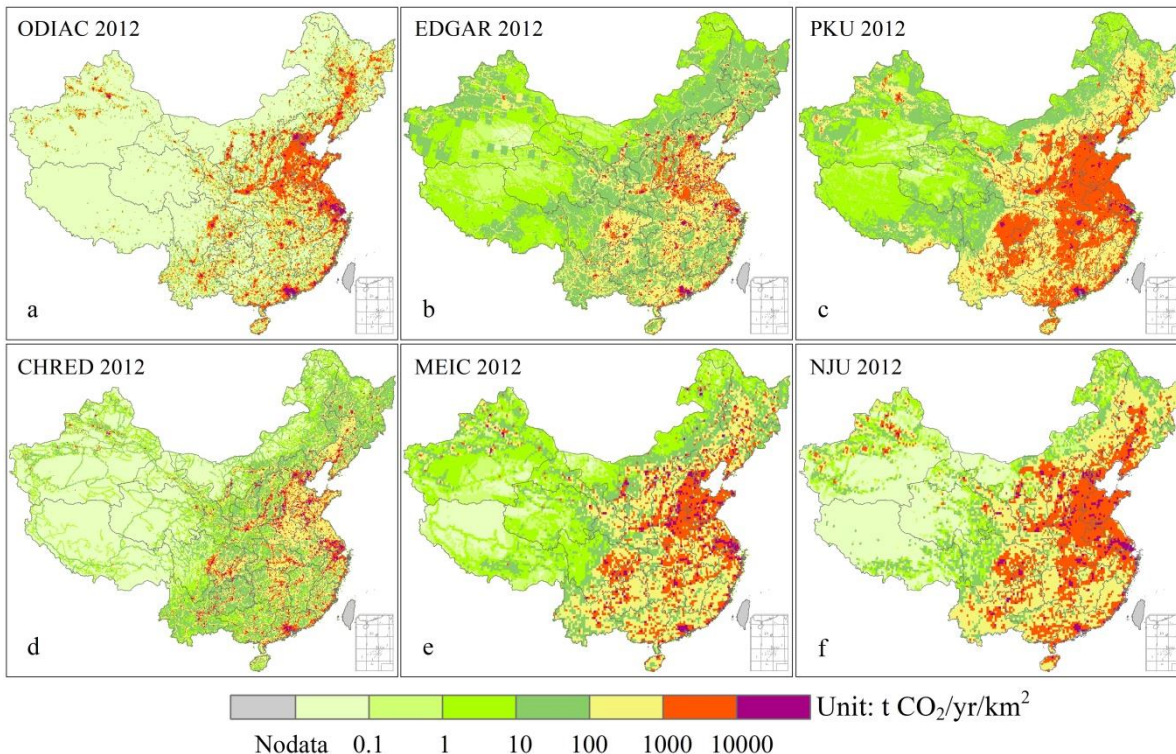
(Guan et al., 2018;Shan et al., 2018). However, there were notable differences among the different estimates at finer spatial scales. Large carbon emissions regions were found in the North China Plain and the Northeast China Plain for ODIAC (Figure 3a), PKU (Figure 3c), MEIC (Figure 3e) and NJU (Figure 3f), which ranged from 1000 to 10,000 t CO₂/km². However, high levels of emissions located in the Sichuan Basin were found from PKU, MEIC and NJU but not from ODIAC.

215 This discrepancy in identifying significant CO₂ emissions was probably due to emissions from rural settlements with high population densities (e.g., Sichuan Basin), which did not appear strongly in satellite nighttime lights or on the ODIAC map (Wang et al., 2013). The more diffusive distributions of MEIC and NJU were attributed to the abundance of point sources, with or without line sources and area sources proxies. Moreover, EDGAR, PKU, CHRED, MEIC and NJU all showed relatively low emissions in western China, but the emissions from ODIAC were zero due to the lack of nighttime light in that

220 region, which tended to distribute more emissions toward strongly lit (at night) urban regions (Wang et al., 2013). EDGAR, CHRED and MEIC all showed traffic line source emissions by inducing traffic networks in the spatial disaggregation. The line emissions (such as expressways, arterial highways) depicted a more detailed spatial distribution in CHRED than in either EDGAR or MEIC. This discrepancy could be attributed to the different road networks and corresponding weighting factors used by each. CHRED disaggregated emissions from the transport sector based on traffic

225 networks and traffic flows (Cai et al., 2018). MEIC applied the traffic network from the China Digital Road-network Map (CDRM) (Zheng et al., 2017), and EDGAR traffic networks were obtained from the OpenStreetMap and OpenRailwayMap (Geofabrik, 2015). ODIAC considered point and area sources while lacking line source emissions in the spatial disaggregation, which places more emissions in populated areas than in suburbs (Oda et al., 2018). Oda and Maksyutov (2011) (Oda and Maksyutov, 2011) noted the possible utility of street lights to represent line source spatial distributions even

230 without the associated specific traffic spatial data. The spatial distributions of traffic emissions are highly uncertain, with biases of 100% or more (Gately et al., 2015), which is largely due to mismatches between the downscaling proxies and the actual vehicle activity distribution.



235 **Figure 3.** Spatial distributions of ODIAC (a), EDGAR (b), PKU (c), CHRED (d), MEIC (e) and NJU (f) at a 10 km resolution for 2012. ODIAC was aggregated from 1 km data, such that MEIC, PKU and EDGAR were resampled from 0.25, 0.1 and 0.1 degrees.

4.3 CO₂ emissions at the provincial level

The provincial level results showed more consistency than the grid level results in terms of spatial distribution. All the products agreed that the eastern and southern provinces were high emitters (>400 Mt CO₂/yr, Figure 4 and S3), while the western provinces were low emitters (<200 Mt CO₂/yr, Figure 4 and S3). The five most emitting provinces were Shandong, Jiangsu, Hebei, Henan and Inner Mongolia, with emissions values ranging from 577 ± 48 Mt to 820 ± 102 Mt CO₂ in 2012 (Figure 4). Meanwhile, the provinces located in the western area with low economic activity and population density showed low carbon emissions (<200 Mt CO₂, Figure 4 and S3). There is a clear discrepancy in the provincial-level emissions among the different estimates, and the mean standard deviation (SD) for the 31 provinces' emissions was 62 Mt CO₂ (or 20%) in 2012. A large SD (>100 Mt CO₂) occurred in high-emitting provinces, such as Shandong, Jiangsu, Inner Mongolia, Shanxi, Hebei and Liaoning. For Shandong Province, the inventories varied from 675-965 Mt CO₂/yr, with a relative SD of 12% (Figure 4 and 5), and for the other high-emitting provinces, the relative SD ranged from 12-48%, which implied that the uncertainty could be further reduced.

Because estimates based on provincial energy statistics are assumed to be more accurate than those derived from the disaggregation of national totals using spatial proxies, we evaluated the provincial emissions of each inventory using the provincial-based inventory mean (CHRED, MEIC, and NJU) (Figure 5). The results showed that emissions derived from the provincial energy statistics are highly correlated, with R-values ranging from 0.99 to 1.00 and slopes ranging 0.96 to 1.04. In contrast, the estimates for ODIAC, EDGAR and PKU, which used IEA national energy statistics, showed an obvious disparity, especially in the five most emitting provinces, suggesting the significant impact of spatial disaggregated approaches in the allocation of total emissions. The potential implication is that when performing spatial disaggregation, national-data-based inventories can use provincial fractions as constraints.

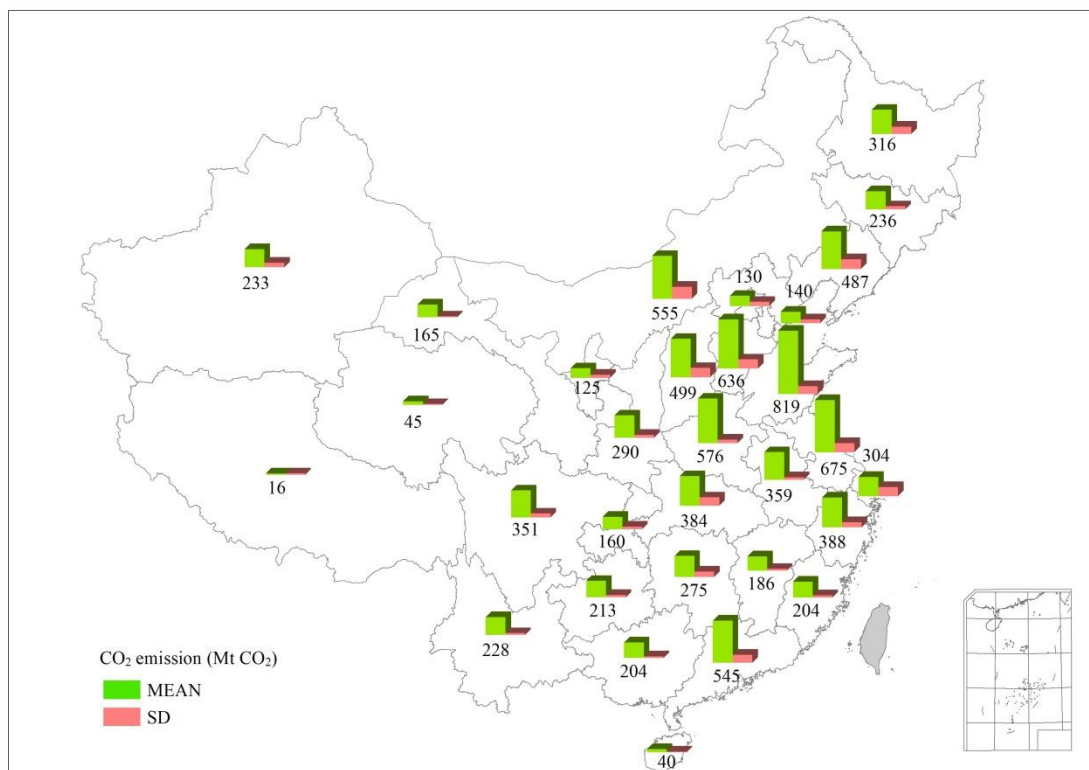
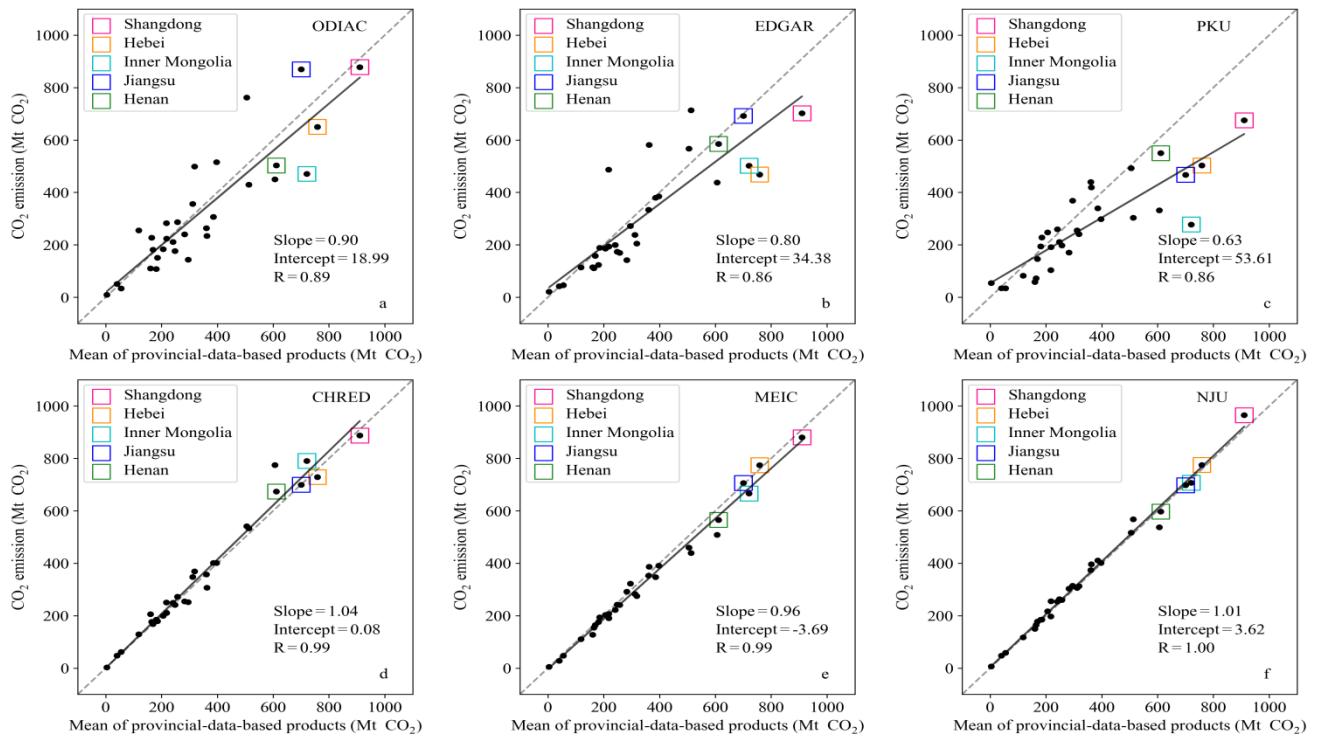


Figure 4. Provincial mean total emissions for ODIAC, EDGAR, PKU, CHRED, MEIC and NJU in 2012. The numbers beneath the green bars are the provincial total CO₂ emissions in Mt.



260

Figure 5. Scatter plots of the provincial total emissions for ODIAC, EDGAR, PKU, CHRED, MEIC and NJU in 2012 with the five most emitting provinces highlighted, and the x-axis is the mean of provincial-data-based products (CHRED, MEIC and NJU).

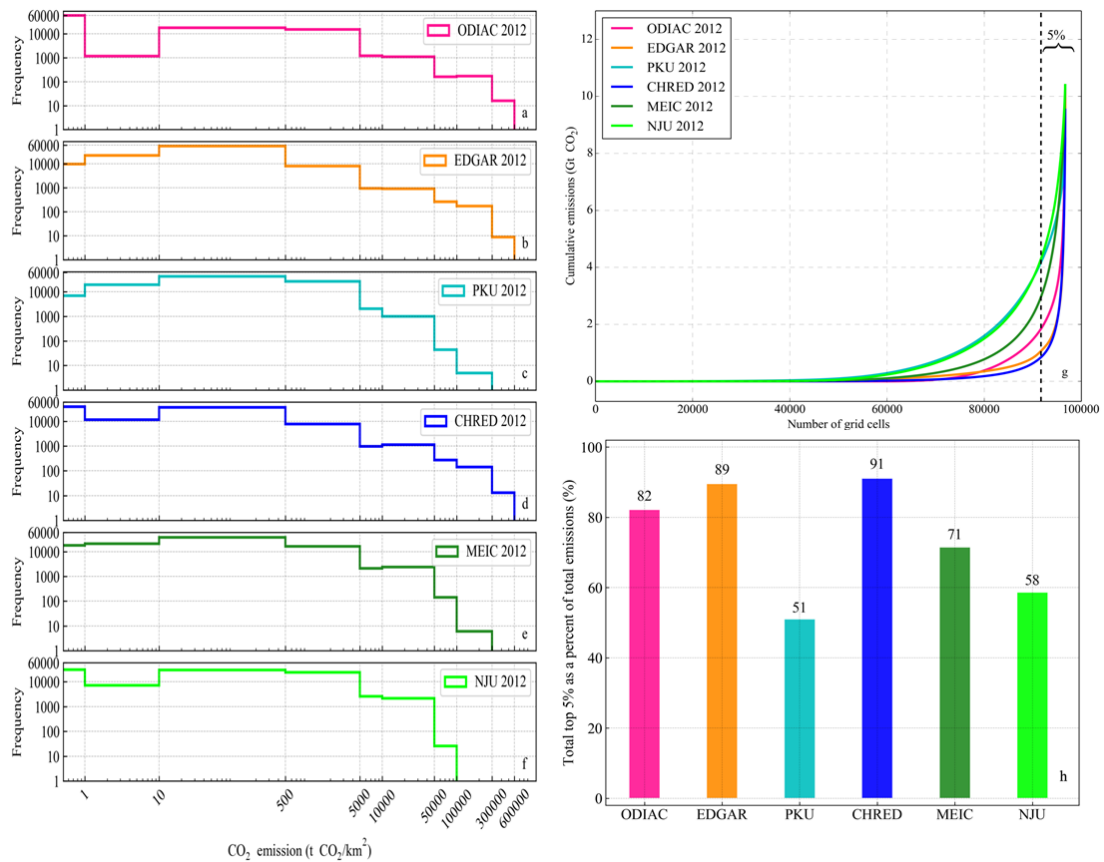
4.4 Statistics of CO₂ emissions at the grid level

To further characterize the spatial pattern of China's CO₂ emissions, the probability density function (PDF), cumulative emissions, and top 5% emitting grids were analyzed to identify the spatial differences from the distribution of grid cell emissions (Figure 6). As illustrated in Figure 4a, ODIAC showed a significant number of cells with zero emissions (62%) (Figure 6a), with medium-emitting grids (500-50,000 t CO₂/km²) constituted 30% and high-emitting grids (>50,000 t CO₂/km²) constituted 3%. Although the low-emissions cells (1-500 t CO₂/km²) were mainly located in EDGAR (58%) and CHRED (69%) (Figure 6b and d) and the medium-emitting grids constituted 30-40%, the high-emitting grids only amounted to 2-3%. This situation could have a significant impact on the cumulative national total emissions (Figure 6g). The frequency distribution of high-emissions grids revealed differences in the point source data. MEIC showed the largest number of high-emitting cells (500-500,000 t CO₂/km², 5% in comparison with the others, which were at 2-3%, Figure 6e) by using a high-resolution emissions database (CPED) that included more power plant information (Li et al., 2017; Liu et al., 2015a). Furthermore, ODIAC and EDGAR agreed well regarding the high emissions (>100,000 t CO₂/km²) because their point source emissions were both from the CARMA database (Table 1). Moreover, CARMA is the only global database that tracks CO₂ that gathers and presents the best available estimates of CO₂ emissions for 50,000 power plants around the world, of

275

which approximately 15,000 have latitude and longitude information with emissions greater than 0. The database includes approximately one-quarter of all greenhouse gas emissions. However, CARMA is no longer active (the last update was November 28, 2012), and the geolocations of power plants are not sufficiently accurate, especially in China (Byers et al., 2019;Liu et al., 2013;Wang et al., 2013;Liu et al., 2015a). Therefore, users must perform corrections themselves (Liu et al., 2013;Oda et al., 2018;Wang et al., 2013;Janssens-Maenhout et al., 2019b;Liu et al., 2015a).

As shown in the cumulative emissions plot (Figure 6g), PKU and NJU showed very similar cumulative curves, and the situation was similar for EDGAR and CHRED. Moreover, the total emissions for EDGAR and CHRED were largely determined by a small proportion of high-emitting grids that showed a steep increase at the last stage of the cumulative curves (Figure 6g), and the top 5% emitting grids accounted for approximately 90% of the total emissions (Figure 6e), which is greater than the comparable values of 82%, 71%, 58% and 51% for ODIAC, MEIC, NJU and PKU, respectively. The emissions from PKU, MEIC and NJU were relatively evenly distributed because CHRED was mainly derived from enterprise-level point sources (Cai et al., 2018). In contrast, the emissions of PKU were the most evenly distributed, and the emissions from the top 5% emitting grids only accounted for 51% (Figure 6g) because PKU incorporated special area source survey data for Chinese rural areas from a 34,489-household energy-mix survey and a 1,670-household fuel-weighting campaign (Tao et al., 2018). Moreover, the use of a spatial disaggregation proxy based on population density also contributed to this spatial pattern. Similarly, MEIC and NJU were evenly distributed because of the same activity data from CESY, National Bureau of Statistics (Table 1).



295 **Figure 6.** Frequency counts (a-f), cumulative emissions (g) (grids are sorted from low to high) and the top 5% emitting grid plots (h) for ODIAC, EDGAR, PKU, CHRED, MEIC and NJU in 2012 at a 10-km resolution.

To identify the locations of hotspots, bubble plots (Figure S2) demonstrated the spatial distribution of high-emitting grid cells that were greater than 50 kt CO₂/km². CHRED, EDGAR and ODIAC showed similar patterns, with high-emitting grids concentrated in city clusters (e.g., Jing-Jin-Ji, the Yangtze River Delta and the Pearl River Delta) and the east coast (Figure S2). EDGAR and ODIAC both derived their power plant emissions from CARMA, but ODIAC was likely to place more emissions than EDGAR over urbanized regions with lights, especially in the North China Plain. The emissions of CPED and CARMA were similar in China, with a minor difference of 2%, although the number of power plants varied significantly (2320 vs. 945) (Liu et al., 2015a), which implied that CARMA tended to allocate similar emissions to fewer plants than CPED.

305 5. Discussion

5.1 Activity data differences in the datasets and their effects

The activity data sources, data level and sectors are the significant determinants of total emissions. As seen in Fig. 1, activity data and EF determine the total emission estimates and affect the spatial distributions by using disaggregation proxies for point, line and area sources. It has been well-discussed that the sum of provincial data is greater than the national total (Guan

310 et al., 2012;Hong et al., 2017;Liu et al., 2015b;Shan et al., 2018;Liu et al., 2013). CEADs (provincial) is 8-18% greater than
CEADs (national) after year 2008 (Figure 2). Thus, the province-based estimates (e.g., NJU and MEIC) are greater than
CEADs (national). This difference could be attributed to the differences in national and provincial statistical systems and
artificial factors, such as the fact that some provincial energy balance sheets were adjusted to achieve an exact match
between supply and consumption (Hong et al., 2017). For example, provincial statistics suffer from data inconsistency and
315 double counting problems (Zhang et al., 2007;Guan et al., 2012). One possible way to improve these statistics is to use the
provincial consumption fractions to rescale the national total consumption when distributing emissions to grids. Hong et al.
(2017) found that the ratio of the maximum discrepancy to the mean value was 16% due to the use of different versions of
national and provincial data in CESY. Ranges of 32-47% of CO₂ emissions from the power sector (mainly coal use) were
found among the inventories, while for the transport sector (mainly liquid fuels), the fractions ranged from 7-9%. Apart from
320 such differences, one peak of FFCO₂ emissions was identified by most datasets in 2013, which were largely found to be due
to slowing economic growth (National Bureau of Statistics, 1998–2017), changes in the industrial structure (Mi et al.,
2017;Guan et al., 2018) and a decline in the share of coal used for energy (Qi et al., 2016). Strategies for reducing emissions
could be based on such uniformed trends, while making reduction policies for provinces requires the support of provincial
energy-based datasets instead of national energy-based datasets.

325 Estimates with more sectors are usually higher than those with fewer sectors. In regard to the incorporation of different
emissions sectors, EDGAR includes international aviation and bunkers (Janssens-Maenhout et al., 2017) and NJU
incorporates waste (Liu et al., 2013) (Table S1), and thus, both were higher than the others. Moreover, for MEIC v.1.3
downloaded from the official website, biofuel combustion (which accounted for approximately 5.7% of the total) was
included; however, the version used here was specially prepared to exclude biofuel to increase the comparability of the
330 database. In addition, CEADs industry processes only include cement production and was thus lower than those (e.g., NJU
and EDGAR) that include more processes (iron and steel, etc.) (Janssens-Maenhout et al., 2017;Shan et al., 2018;Liu et al.,
2013). The PKU dataset used IEA energy statistics with more detailed energy subtypes. The emissions factors were based on
more detailed energy subtypes with lower EFs, while other inventories used the averages of large groups (Table 1), such that
the sum of more detailed subtypes might not equal the total of large groups due to the incompleteness of the statistics. These
335 factors could explain the reasons for the lower emissions estimate (Wang et al., 2013). A further comparison with IEA, EIA
and BP estimates with only energy-related emissions also confirmed that estimates with more sectors would be greater than
those with fewer (Figure S1).

5.2 Effects of emission factors on the total emissions

Carbon emissions are calculated from activity data and EFs, and the uncertainty in estimates is typically reported as 5-10%,
340 while the maximum difference in this study reached 33.8% (or 2.7 PgC) in 2012. One major reason for this difference is the
EF used by these inventories (Table 1). The EF for raw coal ranged from 0.491 to 0.746. For example, CEADs used 0.499 tC

per ton of coal based on large-sample measurements, while EDGAR used 0.713 from the default values recommended by IPCC (Janssens-Maenhout et al., 2017;Liu et al., 2015b;Shan et al., 2018), and the differences were largely due to the low quality and high ash content of Chinese coal. The variability of lignite and coal quality is quite significant. In Liu et al. 345 (2015), the carbon content of lignite ranged from 11-51%, with a mean \pm SD of 28% \pm 13 (n=61). Furthermore, another study showed that the uncertainty from EFs (-16 to 24%) was significantly greater than that from activity data (-1 to 9%) (Shan et al., 2018). We recommended substituting the IPCC default coal EF with the CEADs EF. Regarding plant-level emissions from coal consumption, the collection of EFs measured at fields representing the quality and type of various coals is much-needed to calibrate the large point source emissions, and we call for the inclusion of physical measurements for the 350 calibration and validation of existing datasets (Bai et al., 2007;Dai et al., 2012;Kittner et al., 2018;Yao et al., 2019). Different fuel types contribute differently to emissions factors, i.e., for the same net heating value, natural gas emitted the least amount of carbon dioxide (61.7 kg CO₂/TJ energy), followed by oil (65.3 kg CO₂/TJ energy) and coal (94.6 kg CO₂/TJ energy). Similarly, one successful example for the reduction of air pollutants and CO₂ was that the Chinese government initiated the “project of replacement of coal with natural gas and electricity in North China” in 2016 (Zheng et al., 2018a). Moreover, the 355 nonoxidation fraction of 8% used in Liu et al. (2015) (Liu et al., 2015b) for coal was attributable to the differences when comparing with a default nonoxidation fraction of 0%, as recommended by IPCC (2006) in EDGAR (Janssens-Maenhout et al., 2017). Moreover, the average qualities of coal vary with time, yet we lacked such time-series quality data on raw coal. Bottom-up inventories typically use time-invariant EFs for CO₂ due to the lack of information on coal heating values over time; similarly, the MEIC model also uses constant EFs of CO₂ (Zheng et al., 2018). Teng and Zhu (2015) recommended 360 time-varied conversion factors from raw coal to standard coal, as well as to change the raw coal to commodity coal in energy balance statistics because the latter has relatively efficient statistics on EF.

5.3 Spatial distribution of point, line and area sources

5.3.1 Point sources in datasets and their effects on spatial distribution

Point source emissions account for a large proportion of total emissions (Hutchins et al., 2017). Power plants consumed 365 approximately half of the total coal production in the past decade (Liu et al., 2015a). Thus, the accuracy of point sources was extremely important for improving emission estimates. ODIAC, EDGAR and PKU all distributed power plant emissions from the CARMA dataset. However, the geolocation errors in China are relatively large, and only 45% of power plants are located in the same 0.1 \times 0.1 \circ grid in CARMA v2.0 according to the real power plant locations that were identified by visual inspection in Google maps (Wang et al., 2013). This discrepancy is because CARMA generally treats city-center latitudes 370 and longitudes as the approximate coordinates of power plants (Wheeler and Ummel, 2008;Ummel, 2012).

Liu et al. (2015a) found that CARMA neglected approximately 1300 small power plants in China. Thus, CARMA allocated similar emissions to a more limited number of plants than CPED (Table S2, 720, 1706 and 2320 point sources for ODIAC,

EDGAR and MEIC, respectively), and ODIAC had fewer point sources due to the elimination of incorrect geolocations. The high-emitting grids in CHRED were attributed to the 1.58 million industrial enterprises from the First China Pollution Source Census (FCPSC) that were used as point sources (Wang et al., 2014). Following the CARMA example, we call on the open source of large point sources for datasets and reinforce the importance that Chinese scientists must adjust the locations of point sources from CARMA.

5.3.2 Effects of spatial disaggregation methods on line and area sources

Downscaling methods are widely used because of their uniformity and simplicity due to the lack of detailed spatial data. The disaggregation methods used (e.g., nighttime light, population) by inventories significantly affect the resulting spatial pattern. For example, ODIAC mainly uses nighttime light from satellite images to distribute emissions. Thus, the hotspots concentrate more strongly in high nighttime light regions. However, the use of remote sensing data tends to underestimate industrial and transportation emissions (Ghosh et al., 2010). For instance, coal-fired power plants do not emit strong lights and may be far from cities because transmission lines are used. Electricity generation and use usually occur in different locations, and stronger nighttime light does not always indicate higher CO₂ emissions (Cai et al., 2018; Doll et al., 2000). Furthermore, nighttime lights ignore some other main fossil fuel emissions, such as household cooking with coal. The good correlation between nighttime light and CO₂ emissions is usually on a larger scale basis (national or continental) (Oda et al., 2010; Raupach et al., 2010), while this relationship fails in populated or industrialized rural areas.

Transport networks are also used in several inventories for spatial disaggregation. EDGAR and CHRED both showed clear transport emissions, especially in western China. EDGAR uses three road types and their corresponding weighting factors to disaggregate line source emissions. CHRED uses national traffic networks and their flows to distribute traffic emissions (Cai et al., 2018; Cai et al., 2012). It is easier to obtain traffic networks but rather difficult to obtain traffic flows and vehicle kilometer travelled (VKT) data, and thus, the weighting factors method is significantly easier to apply.

Population is widely used in spatial disaggregation (Andres et al., 2014; Andres et al., 2016; Janssens-Maenhout et al., 2017). CDIAC emissions maps originally used static population data to distribute emissions but have recently changed to a temporally varying population proxy, which has largely reduced uncertainty. However, the unified algorithm for spatial disaggregation, such as the population density approach, encounters difficulties in depicting the uneven development of rural and urban areas, and instead, it usually uses interpolation for a limited number of base years and does not truly vary across years at high spatial resolution (Andres et al., 2014). Furthermore, downscaling approaches may introduce approximately 50% error per pixel, which are spatially correlated (Rayner et al., 2010), a problem that must be considered in future studies.

Moreover, big cities have virtually eliminated the use of coal (Guan et al., 2018; Zheng et al., 2018a), while in rural areas, the use of coal has often increased (Meng et al., 2019). For example, a national survey showed that China's rural residential coal consumption fractions for heating increased from 19.2% to 27.2% (Tao et al., 2018). These transitions have impacts on the spatial distribution of both CO₂ and air pollutants. In addition, the high-resolution CO₂ emissions can serve as a potential

405 proxy for fossil fuel emissions (Wang et al., 2013); thus, further improvements to spatial disaggregation should consider these transitions and the survey data.

410 *Data availability.* The datasets of ODIAC, EDGAR, PKU and CEADs are freely available from <http://db.cger.nies.go.jp/dataset/ODIAC/>, http://edgar.jrc.ec.europa.eu/overview.php?v=432_GHG&SECURE=123, <http://inventory.pku.edu.cn/download/download.html> and <http://www.ceads.net/>, respectively. CHRED, MEIC and NJU are available from the data developers upon request.

415 *Author contributions.* PFH and NZ conceived and designed the study. PFH and XHL collected and analyzed the datasets. PFH, XHL, NZ and TO wrote the paper, with contributions from all the coauthors.

Competing interests. The authors declare that they have no conflict of interest.

420 *Acknowledgments.* This work was supported by the National Key R&D Program of China (No. 2017YFB0504000). We thank Dr. Bofeng Cai from the Chinese Academy for Environmental Planning for kindly providing the CHRED data and his suggestions for improving the manuscript.

425 *Supporting Information.* Data and methodology descriptions of the nine datasets and supplementary figures on emission estimates

426 **References**

- 427 Andres, R. J., Gregg, J. S., Losey, L., Marland, G., and Boden, T. A.: Monthly, global emissions of carbon
428 dioxide from fossil fuel consumption, *Tellus*, 63, 309-327, 2011.
- 429 Andres, R. J., Boden, T. A., Bréon, F. M., and Ciais, P.: A synthesis of carbon dioxide emissions from
430 fossil-fuel combustion, *Biogeosciences*, 9, 1845-1871, 2012.
- 431 Andres, R. J., Boden, T. A., and Higdon, D.: A new evaluation of the uncertainty associated with CDIAC
432 estimates of fossil fuel carbon dioxide emission, *Tellus B: Chemical and Physical Meteorology*, 66,
433 23616, 10.3402/tellusb.v66.23616, 2014.
- 434 Andres, R. J., Boden, T. A., and Higdon, D. M.: Gridded uncertainty in fossil fuel carbon dioxide
435 emission maps, a CDIAC example, *Atmospheric Chemistry & Physics*, 16, 1-56, 2016.
- 436 Bai, X. F., Li, W. H., Chen, Y. F., and Jiang, Y.: The general distributions of trace elements in Chinese
437 coals, *Coal Quality Technology*, 2007.
- 438 Bao, Z., Han, P., Zeng, N., Liu, D., Wang, Y., Tang, G., Yao, B., and Zheng, K.: Observation and modeling
439 of vertical carbon dioxide distribution in a heavily polluted suburban environment, *Atmospheric and
440 Oceanic Science Letters*, 10.1080/16742834.2020.1746627, 2020.
- 441 Berezin, E. V., Konovalov, I. B., Ciais, P., Richter, A., Tao, S., Janssens-Maenhout, G., Beekmann, M., and
442 Schulze, E.-D.: Multiannual changes of CO₂ emissions in China: indirect estimates derived from
443 satellite measurements of tropospheric NO₂ columns, *Atmos. Chem. Phys.*, 13, 9415-9438,
444 <https://doi.org/9410.5194/acp-9413-9415-2013>, 2013.
- 445 Boden, T. A., Marland, G., and Andres, R. J.: Global, Regional, and National Fossil-Fuel CO₂ Emissions,
446 Carbon Dioxide Information Analysis Center, Oak Ridge National Laboratory, U.S. Department of
447 Energy, Oak Ridge, Tenn., USA, https://doi.org/10.3334/CDIAC/00001_V2016, in, 2016.
- 448 Byers, L., Friedrich, J., Hennig, R., Kressig, A., Li, X., McCormick, C., and Malaguzzi, V. L.: A Global
449 Database of Power Plants, in, World Resources Institute. Available online at
450 www.wri.org/publication/global-database-power-plants, Washington, DC, 2019.
- 451 Cai, B., Yang, W., Cao, D., Liu, L., Zhou, Y., and Zhang, Z.: Estimates of China's national and regional
452 transport sector CO₂ emissions in 2007, *Energy Policy*, 41, 474-483, 2012.
- 453 Cai, B., Liang, S., Zhou, J., Wang, J., Cao, L., Qu, S., Xu, M., and Yang, Z.: China high resolution emission
454 database (CHRED) with point emission sources, gridded emission data, and supplementary
455 socioeconomic data, *Resources, Conservation and Recycling*, 129, 232-239,
456 <https://doi.org/10.1016/j.resconrec.2017.10.036>, 2018.
- 457 Dai, S., Ren, D., Chou, C.-L., Finkelman, R. B., Seredin, V. V., and Zhou, Y.: Geochemistry of trace
458 elements in Chinese coals: A review of abundances, genetic types, impacts on human health, and
459 industrial utilization, *International Journal of Coal Geology*, 94, 3-21,
460 <https://doi.org/10.1016/j.coal.2011.02.003>, 2012.
- 461 Doll, C. H., Muller, J.-P., and Elvidge, C. D.: Night-time Imagery as a Tool for Global Mapping of
462 Socioeconomic Parameters and Greenhouse Gas Emissions, *AMBIO: A Journal of the Human
463 Environment*, 29, 157-162, 10.1579/0044-7447-29.3.157, 2000.
- 464 Gately, C. K., Hutyrá, L. R., and Sue Wing, I.: Cities, traffic, and CO₂: A multidecadal assessment of
465 trends, drivers, and scaling relationships, *Proceedings of the National Academy of Sciences*, 112,
466 4999-5004, 10.1073/pnas.1421723112, 2015.
- 467 Geofabrik: Openstreetmap, <https://www.openstreetmap.org> and OpenRailwayMap, 2015.

468 Ghosh, T., Elvidge, C. D., Sutton, P. C., Baugh, K. E., Ziskin, D., and Tuttle, B. T.: Creating a Global Grid of
469 Distributed Fossil Fuel CO₂ Emissions from Nighttime Satellite Imagery, *Energies*, 3, 1895, 2010.

470 Guan, D., Liu, Z., Geng, Y., Lindner, S., and Hubacek, K.: The gigatonne gap in China's carbon dioxide
471 inventories, *Nature Climate Change*, 2, 672-675, 10.1038/nclimate1560, 2012.

472 Guan, D., Meng, J., Reiner, D. M., Zhang, N., Shan, Y., Mi, Z., Shao, S., Liu, Z., Zhang, Q., and Davis, S. J.:
473 Structural decline in China's CO₂ emissions through transitions in industry and energy systems, *Nature*
474 *Geoscience*, 11, 551-555, 10.1038/s41561-018-0161-1, 2018.

475 Han, P., Lin, X., Zeng, N., Oda, T., Zhang, W., Liu, D., Cai, Q. C., Crippa, M., Guan, D., Ma, X.,
476 Janssens-Maenhout, G., Meng, W., Shan, Y., Tao, S., Wang, G., Wang, H., Wang, R., Wu, L., Zhang, Q.,
477 Zhao, F., and Zheng, B.: Province-level fossil fuel CO₂ emission estimates for China based on seven
478 inventories (Accepted), *Journal of Cleaner Production*, 277, 10.1016/j.jclepro.2020.123377, 2020.

479 Hong, C., Zhang, Q., He, K., Guan, D., Li, M., Liu, F., and Zheng, B.: Variations of China's emission
480 estimates: response to uncertainties in energy statistics, *Atmos. Chem. Phys.*, 17, 1227-1239,
481 <https://doi.org/10.5194/acp-1217-1227-2017>, 2017.

482 Hutchins, M. G., Colby, J. D., Marland, G., and Marland, E.: A comparison of five high-resolution
483 spatially-explicit, fossil-fuel, carbon dioxide emission inventories for the United States, *Mitigation and*
484 *Adaptation Strategies for Global Change*, 22, 947.
485 <https://doi.org/910.1007/s11027-11016-19709-11029>, 2017.

486 IEA: Energy Balances of OECD and non-OECD countries, International Energy Agency, Paris, Beyond
487 2020 Online Database, in, 2014.

488 IPCC: IPCC Guidelines for National Greenhouse Gas Inventories. Eggleston, S., Buendia, L., Miwa, K.,
489 Ngara, T., Tanabe, K. (eds.). , IPCC-TSU NGGIP, IGES, Hayama, Japan.
490 www.ipcc-nggip.iges.or.jp/public/2006gl/index.html, 2007.

491 IPCC AR5: IPCC 2013: the physical science basis. Contribution of Working Group I to the Fifth
492 Assessment Report of the Intergovernmental Panel on Climate Change, in, edited by: Stocker, T., Qin,
493 D., Plattner, G., Tignorand, M., Allen, S., Boschungand, J., Nauels, A., Xia, Y., Bex, V., and Midgley, P.,
494 Cambridge University Press, Cambridge, UK, 2013.

495 Janssens-Maenhout, G., Crippa, M., Guizzardi, D., Muntean, M., Schaaf, E., Dentener, F., Bergamaschi,
496 P., Pagliari, V., Olivier, J. G. J., Peters, J. A. H. W., van Aardenne, J. A., Monni, S., Doering, U., and
497 Petrescu, A. M. R.: EDGAR v4.3.2 Global Atlas of the three major Greenhouse Gas Emissions for the
498 period 1970–2012, *Earth Syst. Sci. Data Discuss.*, <https://doi.org/10.5194/essd-2017-5179>, 2017.

499 Janssens-Maenhout, G., Crippa, M., Guizzardi, D., Muntean, M., Schaaf, E., Dentener, F., Bergamaschi,
500 P., Pagliari, V., Olivier, J. G., and Peters, J. A.: EDGAR v4. 3.2 Global Atlas of the three major greenhouse
501 gas emissions for the period 1970–2012, *Earth System Science Data*, 11, 959-1002, 2019a.

502 Janssens-Maenhout, G., Crippa, M., Guizzardi, D., Muntean, M., Schaaf, E., Dentener, F., Bergamaschi,
503 P., Pagliari, V., Olivier, J. G. J., Peters, J. A. H. W., van Aardenne, J. A., Monni, S., Doering, U., Petrescu, A.
504 M. R., Solazzo, E., and Oreggioni, G. D.: EDGAR v4.3.2 Global Atlas of the three major greenhouse gas
505 emissions for the period 1970–2012, *Earth Syst. Sci. Data*, 11, 959-1002, 10.5194/essd-11-959-2019,
506 2019b.

507 Kittner, N., Fadadu, R. P., Buckley, H. L., Schwarzman, M. R., and Kammen, D. M.: Trace Metal Content
508 of Coal Exacerbates Air-Pollution-Related Health Risks: The Case of Lignite Coal in Kosovo,
509 *Environmental Science & Technology*, 52, 2359-2367, 10.1021/acs.est.7b04254, 2018.

510 Le Quéré, C., Andrew, R. M., Friedlingstein, P., Sitch, S., Pongratz, J., Manning, A. C., Korsbakken, J. I.,
511 Peters, G. P., Canadell, J. G., Jackson, R. B., Boden, T. A., Tans, P. P., Andrews, O. D., Arora, V. K., Bakker,

512 D. C. E., Barbero, L., Becker, M., Betts, R. A., Bopp, L., Chevallier, F., Chini, L. P., Ciais, P., Cosca, C. E.,
513 Cross, J., Currie, K., Gasser, T., Harris, I., Hauck, J., Haverd, V., Houghton, R. A., Hunt, C. W., Hurtt, G.,
514 Ilyina, T., Jain, A. K., Kato, E., Kautz, M., Keeling, R. F., Klein Goldewijk, K., Körtzinger, A., Landschützer,
515 P., Lefèvre, N., Lenton, A., Lienert, S., Lima, I., Lombardozzi, D., Metzl, N., Millero, F., Monteiro, P. M. S.,
516 Munro, D. R., Nabel, J. E. M. S., Nakaoka, S.-I., Nojiri, Y., Padin, X. A., Pregon, A., Pfeil, B., Pierrot, D.,
517 Poulter, B., Rehder, G., Reimer, J., Rödenbeck, C., Schwinger, J., Séférian, R., Skjelvan, I., Stocker, B. D.,
518 Tian, H., Tilbrook, B., Tubiello, F. N., van der Laan-Luijkx, I. T., van der Werf, G. R., van Heuven, S., Viovy,
519 N., Vuichard, N., Walker, A. P., Watson, A. J., Wiltshire, A. J., Zaehle, S., and Zhu, D.: Global Carbon
520 Budget 2017, *Earth Syst. Sci. Data*, 10, 405-448, <https://doi.org/410.5194/essd-5110-5405-2018>, 2018.
521 Lei, Y., Zhang, Q., Nielsen, C., and He, K.: An inventory of primary air pollutants and CO₂ emissions
522 from cement production in China, 1990–2020, *Atmospheric Environment*, 45, 147-154,
523 <https://doi.org/10.1016/j.atmosenv.2010.09.034>, 2011.
524 Li, M., Zhang, Q., Kurokawa, J.-I., Woo, J.-H., He, K., Lu, Z., Ohara, T., Song, Y., Streets, D. G., Carmichael,
525 G. R., Cheng, Y., Hong, C., Huo, H., Jiang, X., Kang, S., Liu, F., Su, H., and Zheng, B.: MIX: a mosaic Asian
526 anthropogenic emission inventory under the international collaboration framework of the MICS-Asia
527 and HTAP, *Atmos. Chem. Phys.*, 17, 2017.
528 Liu, F., Zhang, Q., Tong, D., Zheng, B., Li, M., Huo, H., and He, K. B.: High-resolution inventory of
529 technologies, activities, and emissions of coal-fired power plants in China from 1990 to 2010, *Atmos.*
530 *Chem. Phys.*, 15, 13299-13317, 2015a.
531 Liu, M., Wang, H., Oda, T., Zhao, Y., Yang, X., Zang, R., Zang, B., Bi, J., and Chen, J.: Refined estimate of
532 China's CO₂ emissions in spatiotemporal distributions, *Atmos. Chem. Phys.*, 13, 10873-10882,
533 <https://doi.org/10810.15194/acp-10813-10873-12013>, 2013.
534 Liu, Z., Guan, D., Wei, W., Davis, S. J., Ciais, P., Bai, J., Peng, S., Zhang, Q., Hubacek, K., Marland, G.,
535 Andres, R. J., Crawford-Brown, D., Lin, J., Zhao, H., Hong, C., Boden, T. A., Feng, K., Peters, G. P., Xi, F.,
536 Liu, J., Li, Y., Zhao, Y., Zeng, N., and He, K.: Reduced carbon emission estimates from fossil fuel
537 combustion and cement production in China, *Nature*, 524, 335, [10.1038/nature14677](https://doi.org/10.1038/nature14677)
538 <https://www.nature.com/articles/nature14677#supplementary-information>, 2015b.
539 Marland, G., Hamal, K., and Jonas, M.: How Uncertain Are Estimates of CO₂ Emissions?, *Journal of*
540 *Industrial Ecology*, 13, 4-7, 2010.
541 Meng, W., Zhong, Q., Chen, Y., Shen, H., Yun, X., Smith, K. R., Li, B., Liu, J., Wang, X., Ma, J., Cheng, H.,
542 Zeng, E. Y., Guan, D., Russell, A. G., and Tao, S.: Energy and air pollution benefits of household fuel
543 policies in northern China, *Proceedings of the National Academy of Sciences*, 116, 16773,
544 [10.1073/pnas.1904182116](https://doi.org/10.1073/pnas.1904182116), 2019.
545 Mi, Z., Meng, J., Guan, D., Shan, Y., Liu, Z., Wang, Y., Feng, K., and Wei, Y.-M.: Pattern changes in
546 determinants of Chinese emissions, *Environmental Research Letters*, 12, 074003,
547 [10.1088/1748-9326/aa69cf](https://doi.org/10.1088/1748-9326/aa69cf), 2017.
548 National Bureau of Statistics: China Statistical Yearbook 1998–2016, China Statistics Press, 1998–2017.
549 National Bureau of Statistics: China Energy Statistical Yearbook 2016, China Statistics Press, Beijing,
550 2016.
551 NDRC: The People's Republic of China Second National Communication on Climate Change,
552 <http://ghs.ndrc.gov.cn/zcfg/201404/W020140415316896599816.pdf>, 2012a.
553 NDRC: Guidelines for China's Provincial GHG Emission Inventories, in, 2012b.
554 Oda, T., Maksyutov, S., and Elvidge, C. D.: Disaggregation of national fossil fuel CO₂ emissions using a
555 global power plant database and DMSP nightlight data, *Proc. of the 30th Asia-Pacific Advanced*

556 Network Meeting, 220–229, 2010.

557 Oda, T., and Maksyutov, S.: A very high-resolution (1 km×1 km) global fossil fuel CO₂ emission
558 inventory derived using a point source database and satellite observations of nighttime lights, *Atmos.*
559 *Chem. Phys.*, 11, 543-556, <https://doi.org/510.5194/acp-5111-5543-2011>, 2011.

560 Oda, T., Maksyutov, S., and Andres, R. J.: The Open-source Data Inventory for Anthropogenic CO₂,
561 version 2016 (ODIAC2016): a global monthly fossil fuel CO₂ gridded emissions data product for tracer
562 transport simulations and surface flux inversions, *Earth Syst. Sci. Data*, 10, 87-107,
563 <https://doi.org/110.5194/essd-5110-5187-2018>, 2018.

564 Olivier, J. G. J., Janssens - Maenhout, G., Muntean, M., and Peters, J. A. H. W.: Trends in global CO₂
565 emissions: 2014 report, JRC93171/PBL1490 report, ISBN: 978-994-91506-91587-91501, 2014.

566 Qi, Y., Stern, N., Wu, T., Lu, J., and Green, F.: China's post-coal growth, *Nature Geoscience*, 9, 564-566,
567 10.1038/ngeo2777, 2016.

568 Qin, D., Ding, Y., and Mu, M.: Climate and Environmental Change in China: 1951–2012, in: Springer
569 Environmental Science & Engineering, edited by: Qin, D., Ding, Y., and Mu, M., Springer-Verlag Berlin
570 Heidelberg 2016, 2016.

571 Raupach, M. R., Rayner, P. J., and Paget, M.: Regional variations in spatial structure of nightlights,
572 population density and fossil-fuel CO₂ emissions, *Energy Policy*, 38, 4756-4764,
573 <https://doi.org/10.1016/j.enpol.2009.08.021>, 2010.

574 Rayner, P. J., Raupach, M. R., Paget, M., Peylin, P., and Koffi, E.: A new global gridded data set of CO₂
575 emissions from fossil fuel combustion: Methodology and evaluation, *Journal of Geophysical Research*
576 *Atmospheres*, 115, doi:10.1029/2009JD013439, 2010.

577 SCIO, T. S. C. I. O. o. C.: Enhanced Actions on Climate Change: China's Intended Nationally Determined
578 Contributions,
579 [http://www.scio.gov.cn/xwfbh/xwfbh/wqfbh/33978/35364/xgzc35370/Document/1514539/1514539](http://www.scio.gov.cn/xwfbh/xwfbh/wqfbh/33978/35364/xgzc35370/Document/1514539/1514539.htm)
580 [9.htm](http://www.scio.gov.cn/xwfbh/xwfbh/wqfbh/33978/35364/xgzc35370/Document/1514539/1514539.htm), 2015.

581 Shan, Y., Liu, J., Liu, Z., Xu, X., Shao, S., Wang, P., and Guan, D.: New provincial CO₂ emission
582 inventories in China based on apparent energy consumption data and updated emission factors,
583 *Applied Energy*, 184, 2016.

584 Shan, Y., Guan, D., Zheng, H., Ou, J., Li, Y., Meng, J., Mi, Z., Liu, Z., and Zhang, Q.: China CO₂ emission
585 accounts 1997-2015, *Scientific Data*, 5, 170201, 2018.

586 Tao, S., Ru, M. Y., Du, W., Zhu, X., Zhong, Q. R., Li, B. G., Shen, G. F., Pan, X. L., Meng, W. J., Chen, Y. L.,
587 Shen, H. Z., Lin, N., Su, S., Zhuo, S. J., Huang, T. B., Xu, Y., Yun, X., Liu, J. F., Wang, X. L., Liu, W. X., Cheng,
588 H. F., and Zhu, D. Q.: Quantifying the rural residential energy transition in China from 1992 to 2012
589 through a representative national survey, *Nature Energy*, 3, 567-573, 10.1038/s41560-018-0158-4,
590 2018.

591 Teng, F., and Zhu, S.: Which estimation is more accurate? A technical comments on Nature Paper by
592 Liu et al on overestimation of China's emission, *Science & Technology Review*, 33, 112-116, 2015.

593 Ummel, K.: Carma Revisited: An Updated Database of Carbon Dioxide Emissions from Power Plants
594 Worldwide, Working Papers, 2012.

595 Wang, J., Cai, B., Zhang, L., Cao, D., Liu, L., Zhou, Y., Zhang, Z., and Xue, W.: High resolution carbon
596 dioxide emission gridded data for China derived from point sources, *Environmental Science &*
597 *Technology*, 48, 7085-7093, 2014.

598 Wang, M., and Cai, B.: A two-level comparison of CO₂ emission data in China: Evidence from three
599 gridded data sources, *Journal of Cleaner Production*, 148, 194-201,

600 <https://doi.org/10.1016/j.jclepro.2017.02.003>, 2017.

601 Wang, R., Tao, S., Ciais, P., Shen, H. Z., Huang, Y., Chen, H., Shen, G. F., Wang, B., Li, W., Zhang, Y. Y., Lu,
602 Y., Zhu, D., Chen, Y. C., Liu, X. P., Wang, W. T., Wang, X. L., Liu, W. X., Li, B. G., and Piao, S. L.:
603 High-resolution mapping of combustion processes and implications for CO₂ emissions, *Atmos. Chem.*
604 *Phys.*, 13, 5189-5203, <https://doi.org/5110.5194/acp-5113-5189-2013>, 2013.

605 Wheeler, D., and Ummel, K.: Calculating CARMA: Global Estimation of CO₂ Emissions from the Power
606 Sector, Working Papers, 2008.

607 Yao, B., Cai, B., Kou, F., Yang, Y., Chen, X., Wong, D. S., Liu, L., Fang, S., Liu, H., Wang, H., Zhang, L., Li, J.,
608 and Kuang, G.: Estimating direct CO₂ and CO emission factors for industrial rare earth metal
609 electrolysis, *Resources, Conservation and Recycling*, 145, 261-267,
610 <https://doi.org/10.1016/j.resconrec.2019.02.019>, 2019.

611 Zeng, N., Ding, Y., Pan, J., Wang, H., and Gregg, J.: Climate Change--the Chinese Challenge, *Science*,
612 319, 730-731, 10.1126/science.1153368, 2008.

613 Zhang, Q., Streets, D. G., He, K., and Klimont, Z.: Major components of China's anthropogenic primary
614 particulate emissions, *Environmental Research Letters*, 2, 045027, 2007.

615 Zheng, B., Zhang, Q., Tong, D., Chen, C., Hong, C., Li, M., Geng, G., Lei, Y., Huo, H., and He, K.:
616 Resolution dependence of uncertainties in gridded emission inventories: a case study in Hebei, China,
617 *Atmos. Chem. Phys.*, 17, <https://doi.org/10.5194/acp-17-921-2017>, 2017.

618 Zheng, B., Tong, D., Li, M., Liu, F., Hong, C., Geng, G., Li, H., Li, X., Peng, L., Qi, J., Yan, L., Zhang, Y., Zhao,
619 H., Zheng, Y., He, K., and Zhang, Q.: Trends in China's anthropogenic emissions since 2010 as the
620 consequence of clean air actions, *Atmos. Chem. Phys.*, 18, 14095-14111,
621 <https://doi.org/14010.15194/acp-14018-14095-12018>, , 2018a.

622 Zheng, B., Zhang, Q., Davis, S. J., Ciais, P., Hong, C., Li, M., Liu, F., Tong, D., Li, H., and He, K.:
623 Infrastructure Shapes Differences in the Carbon Intensities of Chinese Cities, *Environmental Science &*
624 *Technology*, 52, 6032-6041, 10.1021/acs.est.7b05654, 2018b.

625

626